

Article

Selective Detection of Liquid Viscosity Using Acoustic Plate Waves with In-Plane Polarization

Vladimir Anisimkin ¹, Elizaveta Shamsutdinova ¹ , Peng Li ², Bin Wang ², Feng Zhu ², Zhenghua Qian ^{2,*} 
and Iren Kuznetsova ^{1,*} 

¹ Kotelnikov Institute of Radio Engineering and Electronics of RAS, 125009 Moscow, Russia; anis@cplire.ru (V.A.); shes1996@bk.ru (E.S.)

² State Key Laboratory of Mechanics and Control of Mechanical Structures, College of Aerospace Engineering, Nanjing University of Aeronautics and Astronautics, Nanjing 210016, China; lipeng_mech@nuaa.edu.cn (P.L.); wangbin1982@nuaa.edu.cn (B.W.); zhufeng.phd@nuaa.edu.cn (F.Z.)

* Correspondence: qianzh@nuaa.edu.cn (Z.Q.); kuziren@yandex.ru (I.K.)

Abstract: Using plates of weak piezoelectric crystal (quartz) loaded with various liquids, it is shown that along with common modes, whose sensitivity towards different liquid parameters comparable with each other, there are some uncommon modes, whose amplitude responses towards viscosity η are much larger than towards temperature T and electric conductivity σ . The search of the modes with the selective properties is accomplished by varying plate thickness h , crystal orientation, wave length λ , and mode order n . It is found that all modes possessing the property are characterized by small surface-normal displacement, avoiding wave radiation into adjacent liquid, large in-plane displacements, enhancing viscous coupling the modes and liquids, and small electro-mechanical constant, reducing electro-acoustic interaction. Basing on the modes, the sensor prototypes with selective operation are developed and tested for η from 1 to 1500 cP, σ from 0 to 1.2 S/m, and t from 0 to 55 °C. Because of operation at ultrasonic frequency (tens MHz) the prototypes have different sensitivities in various η -ranges: 0.3 dB/cP for 1–20 cP, 0.12 dB/cP for 20–100 cP, and 0.015 dB/cP for 100–1500 cP. Viscosity responses of the prototypes become comparable with their electric outputs only for $\eta < 2$ cP. Temperature responses are almost zero in air, but when plate is coated with liquid they increase depending on liquid properties, allowing measurements of the temperature dependence of the liquid viscosity.

Keywords: liquid viscosity; conductivity; temperature; piezoelectric plate; acoustic plate wave; attenuation



Citation: Anisimkin, V.; Shamsutdinova, E.; Li, P.; Wang, B.; Zhu, F.; Qian, Z.; Kuznetsova, I. Selective Detection of Liquid Viscosity Using Acoustic Plate Waves with In-Plane Polarization. *Sensors* **2022**, *22*, 2727. <https://doi.org/10.3390/s22072727>

Academic Editor: Antonio Lázaro

Received: 5 March 2022

Accepted: 30 March 2022

Published: 1 April 2022

Publisher's Note: MDPI stays neutral with regard to jurisdictional claims in published maps and institutional affiliations.



Copyright: © 2022 by the authors. Licensee MDPI, Basel, Switzerland. This article is an open access article distributed under the terms and conditions of the Creative Commons Attribution (CC BY) license (<https://creativecommons.org/licenses/by/4.0/>).

1. Introduction

The measurement of fluid viscosity is an important problem for various applications in some industries (machine, instrument, chemical, food, pharmaceutical), agriculture, bio-engineering, ecology, etc. [1–7]. The knowledge on viscosity is also necessary in medicine for characterizing rheological bio-liquids (blood, sperm) [8]. To measure this parameter a need was recognized for microsensing devices with small size, high precision, good reliability, and multiple usages. One of the most attractive approaches for developing such sensors is the use of acoustic wave propagation [9]. Acoustic devices are relay upon the changes in the wave amplitude and velocity when a sample of liquid loads propagation medium [10]. The acoustic sensors are potentially attractive because they do not require large fluid samples, do not introduce significant distortions into the probe, allow remote data collection via radio channel, and have two independent responses (phase and amplitude) to each action. Performance of the sensors depends evidently on the type of acoustic wave exploited in device. Till now Rayleigh surface acoustic waves (SAW) [10,11], shear-horizontal (SH) SAW [12–15], leaky SAW [16], bulk acoustic waves [17–20], slot acoustic wave [21], SH plate acoustic waves (PAW) of zero order [22],

and PAW of higher order propagating in isotropic [23,24] and piezoelectric [25–30] and plates were used for the purpose. The resonators with a lateral electric field excitation have recently been suggested for measurement conductivity and viscosity of liquids [31]. For this purpose it is possible to use new structures like phononic crystals with various periodic inclusions as well [32–34].

Recently, new modification of the Lamb waves was found [35]. It has small vertical displacement accompanied with large shear-horizontal and longitudinal components, i.e., elliptic polarization parallel to the plate faces. The modified wave generated at 49.74 MHz in ST,X-quartz plate with normalized plate thickness $h/\lambda = 1.0$ (h —thickness, λ —wave length) responds strongly on glycerin loading (viscosity $\eta = 1490$ cP), thereby demonstrating high sensitivity towards fluid viscosity.

In general, most acoustic sensors are based on common delay lines with input and output interdigital transducers (IDTs) and test liquid located between them. Usually, most modes propagating in crystal plates with liquid loadings are sensitive to different liquid parameters more or less equally [9]. As a result, in order to measure a single parameter alone, special sensor configurations, several independent measurements, and relevant signal processing are required [29,30]. This property brings up the question: are there acoustic waves, whose partial response towards one liquid parameter (e.g., viscosity η) is much larger than towards others (e.g., temperature T and electric conductivity σ). If so, selectivity of the wave will provide direct measuring relevant liquid parameter without any special configurations and signal processing.

The goal of the present paper is to study this question basing on quartz plates and various acoustic plate modes including new modification. Theoretical and experimental analysis of the waves is accomplished for fluids with different viscosities and electric conductivities.

2. Materials and Methods

2.1. Theoretical Methods

Let us consider an acoustic wave, propagating along x_1 direction in a piezoelectric plate (Figure 1a). In order to find phase velocity and mechanical displacements of the wave the equation of motion, Laplace's equation, material equations for electric displacement and mechanical stress are used for plate medium, while Laplace's equation and equation for electric induction are used for vacuum. Then, relevant electric and mechanical conditions on vacuum/plate boundary are considered, and boundary condition matrix was formed. The value of wave velocity v_n is found using iterative search procedure by zeroing determinant of the matrix. After that three partial components of mechanical displacement (u_1, u_2, u_3) are calculated for as-found value of velocity v_n at any depth x_3 of the plate [36].

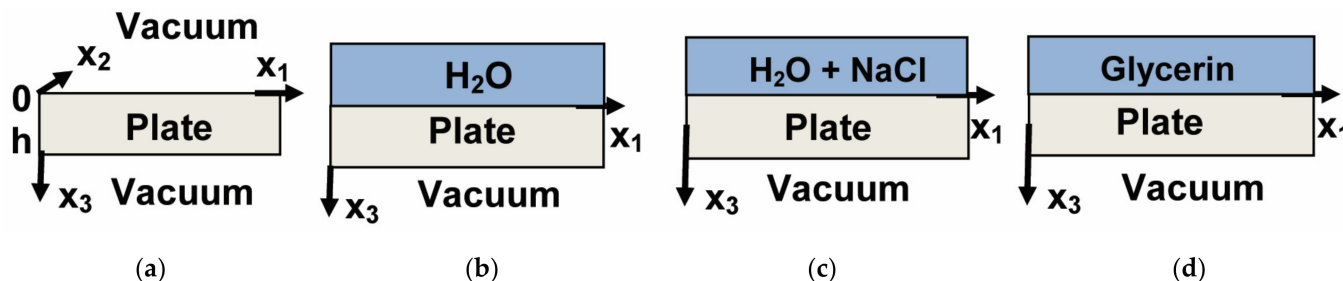


Figure 1. Geometry of the problems: structure “vacuum-plate-vacuum” (a), structure “vacuum-plate- H_2O ” (b), structure “vacuum-plate- water solution with NaCl” (c), and structure “vacuum-plate-glycerin” (d).

When a plate is loaded with semi-infinite not viscose, not conductive liquid (Figure 1b) the equation of motion, Laplace's equation, material equations for electric displacement and mechanical stress are used for the liquid. The liquid/plate boundary conditions are the

continuity of the normal mechanical displacement ($u_3^{pl} = u_3^{lq}$), normal mechanical stress ($T_{33}^{pl} = T_{33}^{lq}$), electric displacement ($D_{33}^{pl} = D_{33}^{lq}$), and electric potential ($\Phi^{pl} = \Phi^{lq}$) [37].

When a plate is loaded with semi-infinite non viscose, but conductive liquid (Figure 1c) Poisson's equation instead of Laplace's equation is used for liquid, while equation for continuity of electric charge, material equation for current, and condition of zero electric current are added to the plate/liquid boundary conditions [22].

When a plate is loaded with semi-infinite viscose, but nonconductive liquid (Figure 1d) Laplace's equation instead of Poisson's equation is used, while continuity of all mechanical displacements, mechanical stress, electric displacement, and electric potential are taken as boundary conditions. In this case, viscosity of the liquid is accounted as imaginary part $i\omega\eta_{ij}$ of elastic moduli, where i is imaginary value, $\omega = 2\pi f$ is circular frequency, η_{ij} are viscosity coefficients in $\text{Pa} \times \text{s}$ [22].

Material constants of quartz, distilled H_2O , and glycerin are taken from [38–40] and presented in Table 1.

Table 1. Density ρ (kg/m^3), elastic constants C_{ij} (GPa), piezoelectric coefficients e_{ij} (C/m^2), viscosity coefficients η_{ij} ($\text{Pa} \times \text{s}$) and dielectric permittivity ϵ_{ij}/ϵ_0 of quartz, distilled H_2O and glycerin used in calculations ($T = 22.5^\circ\text{C}$).

Quartz													
ρ	C_{11}^E	C_{12}^E	C_{13}^E	C_{14}^E	C_{24}^E	C_{33}^E	C_{44}^E	C_{66}^E	e_{11}	e_{12}	e_{14}	ϵ_{11}/ϵ_0	ϵ_{33}/ϵ_0
2650	86.7	7	11.9	−17.9	17.9	107	57.9	39.85	0.171	−0.171	−0.0406	4.4	4.6
H ₂ O							Glycerin						
ρ	C_{11}	ϵ/ϵ_0	ρ	C_{11}	η_{11}	C_{44}	η_{44}	ϵ/ϵ_0					
997.299	2.25	80	1260	2.81	118.6	1.2128×10^{-3}	1.5	41.9					

2.2. Experimental Methods

The measurements are carried out at room temperature and atmospheric pressure. The plates of ST-quartz with Euler angles $0^\circ, 132.75^\circ, 0^\circ$ and $0^\circ, 132.75^\circ, 90^\circ$ are used as a weak piezoelectric material. The normalized thickness of the plates are $h/\lambda = 0.6, 1.0, 1.25, 1.485,$ and 1.67 ($h = 300$ and $500 \mu\text{m}$, $\lambda = 200, 202, 300, 400$ and $500 \mu\text{m}$), providing variety of the modes for analysis [35,41,42]. The plates have one grinded (top) and one polished (bottom) surface. The top surface is sealed with a liquid cell (fused quartz) which is large enough to avoid perturbation of an acoustic beam by the cell. The bottom surface contains three pairs of interdigital transducers (IDTs) having periodical structure. Two pairs of identical transducers with periods $\lambda = 200, 202, 300, 400$ or $500 \mu\text{m}$ are aligned perpendicular each other (Figure 2a). Details of the test samples which are sufficient for reproducing experimental results are presented in Table 2. The 1st pair is used to generate generalized Lamb modes along X-axis (Euler angles $0^\circ, 132.75^\circ, 0^\circ$); the 2nd pair excites shear-horizontal (SH) modes perpendicular to X-axis ($0^\circ, 132.75^\circ, 90^\circ$); the 3rd pair of small transducers with period $\lambda = 20 \mu\text{m}$ is intended for controlling the plate and liquid temperature T by surface acoustic waves: the change ΔT , if any, is detected as $\Delta T = (\text{TCD})^{-1} \times \Delta\varphi/\varphi$, where $\Delta\varphi/\varphi$ is the change in the phase of the wave and TCD is the wave temperature coefficient [43]. Each transducer comprises of 20 finger electrodes patterned from 1000-nm-thick Cr/Al. The large number of electrodes provides good frequency resolution for neighboring acoustic plate modes with close velocities v_n .

The measurements of the insertion loss $S_{12}(f)$ are carried out using KEYSIGHT 5061B network analyzer (Keysight, Santa Rosa, CA, USA) operating in amplitude-frequency format (Figure 2a). In order to avoid an influence of electromagnetic leakage the amplitude-frequency format $S_{12}(f)$ is converted to the amplitude-time format $S_{12}(\tau)$, where the gate window is started just after the leakage and stopped after acoustic signal. When the gate is on, the leakage is off and the time delay format $S_{12}(\tau)$ converted back to the frequency format $S_{12}(f)$ without the leakage (Figure 3).

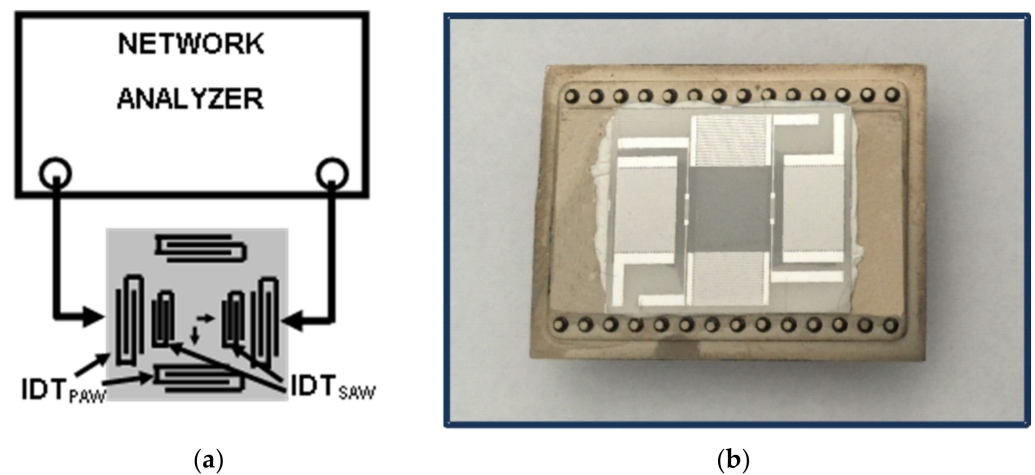


Figure 2. Schematic view (a) and photo (b) of a test sample with interdigital transducers generating Lamb and SH (PAW), and surface (SAW) acoustic waves.

Table 2. The characteristics of the test samples.

IDT Period λ , μm	IDT Aperture, μm	Number of Electrode Pairs	Face-to-Face Distance, μm
200, 202	5500	20	8500
300	9000	20	16,000
400	10,400	20	17,600
500	13,000	20	22,000
20	1600	20	8000

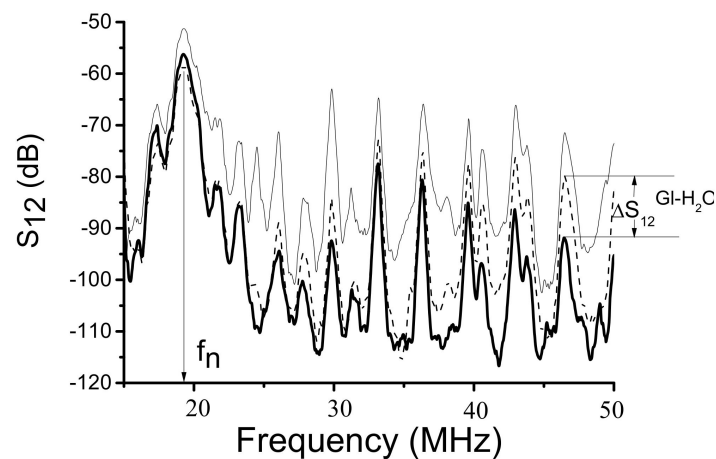


Figure 3. Typical insertion loss S_{12} measured in ST,X-quartz plate with two free faces (thin solid), one free face and one water-loaded face (dashed), and one free face and one glycerin-loaded face (thick solid). Plate: $h = 500 \mu\text{m}$, IDTs: $\lambda = 300 \mu\text{m}$, $h/\lambda = 1.67$. Liquids are over the propagation path $L = 22 \text{ mm}$ on the bottom of the plate.

The mode velocities are measured as $v_n = \lambda \times f_n$, where λ is period of IDTs (the wavelength), f_n is the central frequency of the modes (Figure 3). Precision of the measurements is $\pm 1\%$.

The measurement of the attenuation coefficient α_n produced by a liquid is carried out also using KEYSIGHT 5061B network analyzer (Keysight, Santa Rosa, CA, USA) (Figure 2). For each mode n the value of the insertion loss S_{12}^{air} is, first, measured in air (without

liquid) at relevant frequency $f_n = v_n/\lambda$ (Figure 3). Second, the same loss $S_{12}^{H_2O}$, $S_{12}^{H_2O+Gl}$, and S_{12}^{Gl} are recorded after distilled water (viscosity $\eta = 1.003$ cP), water solutions of glycerin (1.003 cP $< \eta < 1491$ cP) and pure glycerin ($\eta = 1491$ cP) are introduced into the cell one by one as liquids with variable viscosity, zero electric conductivity $\sigma = 0$ and slightly varied density ($<26\%$) and permittivity ($<10.5\%$) [39]. Third, the attenuation coefficient α_n for each mode and test liquid is deduced as $\alpha_n = (S_{12}^{Gl} - S_{12}^{H_2O})/L = \Delta S_{12}^{(Gl-H_2O)}/L$, where L is a propagation path of a mode along a liquid. Finally, for each sample the modes n with largest α_n are determined and compared with one another. Precisions of the measurements are ± 0.01 dB for S_{12} and ± 0.005 dB/mm for α_n .

In order to measure sensitivity of the modes towards liquid conductivity σ the water solutions of NaCl with σ varied from 0 (distilled water) to 10 S/m (7.6 weight % NaCl in water) are used as test liquids with almost constant viscosity ($<13\%$), density ($<8\%$), and permittivity ($<1\%$) [39].

Taking into account strong dependence of liquid properties on the temperature T , most measurements are carried out at 20 ± 0.1 °C fixed by thermal camera UC-20CE (NOSELAB ATS, Nova Milanese, Italy). On the other hand, in order to study the temperature sensitivity of the sensor the camera is heated from $T = 0$ to 55 °C with the step $\Delta T = 5$ °C and same measurements for each temperature are accomplished without any liquid and with water and glycerin. When a liquid is absent the sensor slightly responds to temperature according to properties of the wave ($S_{12}^{air} \sim 0.1$ dB). When a liquid is present, the response of the sensor is additionally depends on the value of liquid viscosity at relevant temperature. So that, by extracting 1st set of data from the 2nd gives us the temperature dependence of viscosity $\eta(T)$ for a given liquid. Precision of the measurements is $\pm 20\%$.

All liquid solutions are prepared by mixing partial components in forced vibrator for about 5 min. Knowing the components weights, the values η and σ at 20 °C are found from [39]. An error in weight concentration of glycerin and NaCl in water is about $\pm 1\%$.

The volumes of the test liquids sufficient for making measurements are about 100 μ L.

3. Results and Discussion

Table 3 shows results of the calculations for higher-order modes propagating in quartz plates with two free faces and plates with one free, one liquid loaded face. It is seen that (i) mode 1 of the Table 3 has dominant u_3^0 component ($u_3^0 \gg u_1^0, u_2^0$) and, thereby, large radiation loss into the liquid; (ii) modes 3 and 4 possess dominant shear-horizontal components ($u_2^0 \gg u_1^0, u_3^0$) and, therefore, the attenuation of the modes is not originated from radiation, but from relaxation process related with liquid viscosity. The modes of this type has recently been used for viscosity sensors [22,25–27]; (iii) mode 2 has small vertical displacement, large shear-horizontal and large longitudinal components, i.e., elliptic polarization which is oriented parallel to the plate faces ($u_1^0, u_2^0 \gg u_3^0$), the polarization being maintained for any loading. So that, the mode 2 is just the modified Lamb wave [35]. The attenuation of the mode is originated from viscous coupling. The electromechanical coupling coefficient of the mode 2 is small ($k^2 = 0.02\%$).

Total amount of modes detected in 9 quartz plates is as large as 100. Most of them are not suited for application because of too large attenuation arising from (i) compression wave radiation into adjacent liquid (proportional to surface-normal component u_3), and (ii) viscous coupling the modes and liquid (proportional to in-plane components u_1 and u_2). Nevertheless, the modes with allowable attenuation are found in the plates though the liquid-loaded loss for some modes approaches 100 dB (Table 4, last column).

Best modes belonging to SH and Lamb families and propagating in different plates are presented in Table 4. The mode responses towards glycerin referred to responses for water are as large as $\Delta\alpha_n^{(Gl-H_2O)} = 1.08\text{--}1.64$ dB/mm (bold).

Table 3. The velocities v_{ph} , normalized displacements u_1^0, u_2^0, u_3^0 at $x_3 = 0$ and attenuation coefficients α_n of APM in quartz plates with two free faces and plates with one free–one liquid loaded faces. Plates: ST,X and ST,X + 90°-quartz with $h/\lambda = 1$. Loadings: distilled H₂O, water solution of NaCl (conductivity $\sigma = 0.24$ S/m), and pure glycerin (viscosity $\eta = 1491$ cP).

#	Plate, Frequency	Free Plate v_n , m/s ($u_1^0; u_2^0; u_3^0$) α_n , dB/mm	Plate + H ₂ O v_n , m/s ($u_1^0; u_2^0; u_3^0$) α_n , dB/mm	Plate + H ₂ O + NaCl v_n , m/s ($u_1^0; u_2^0; u_3^0$) α_n , dB/mm	Plate + Glycerin v_n , m/s ($u_1^0; u_2^0; u_3^0$) α_n , dB/mm
1	ST,X-Quartz $f_n = 48.5$ MHz	14,529.277 (1; 9.2; 130) 0	14,528.546 (1; 2.8; 41) 1	14,528.52 (1; 2.9; 41) 1	disappeared
2	ST,X-Quartz $f_n = 49.74$ MHz	14,956.63 (1; 1.6; 0.007) 0	14,955.982 (1; 1.6; 0) 6.6×10^{-6}	14,955.96 (1; 1.6; 0) 2.8×10^{-4}	14,927.698 (1; 1.6; 0.015) 0.33
3	ST,X + 90°-Quartz $f_n = 53.48$ MHz	16,058.053 (1; 77,000; 0.15) 0	16,057.432 (1; 77,381; 0.15) 0	16,057.41 (1; 77,427; 0.15) 5×10^{-5}	16,027.35 (1; 75,689; 0.14) 0.33
4	ST,X + 90°-Quartz $f_n = 58.87$ MHz	17,676.182 (1; 68,700; 0.55) 0	17,675.604 (1; 72,613; 0.55) 0	17,675.587 (1; 72,893; 0.55) 2×10^{-4}	17,644.028 (1; 52,615; 0.6) 0.3

Table 4. Acoustic plate modes with largest responses towards viscosity measured in different quartz plates at 20 °C.

Plate	h/λ	f_n , MHz	L, mm	$\Delta S_{12}(GI-H_2O)$, dB	$\alpha_n(GI-H_2O)$, dB/mm	$S_{12}(GI)$, dB
ST,X-Quartz	0.6	19.95	20	22.9	1.15	94.6
ST,X + 90°-Quartz	0.6	19.88	20	10	0.5	74.2
ST,X-Quartz	1.0	49.74	22	27	1.23	79.6
ST,X + 90°-Quartz	1.0	53.48	22	34	1.55	100.5
ST,X + 90°-Quartz	1.25	34.26	30	13.9	0.46	89.4
ST,X-Quartz	1.485	28.85	31	23.6	0.76	72.1
ST,X + 90°-Quartz	1.485	46.36	31	33.5	1.08	94
ST,X-Quartz	1.67	47.1	22	17.5	0.8	−91.9
ST,X + 90°-Quartz	1.67	46.73	22	20	0.9	−81.3

Examples of the best modes are shown on Figure 4 ($f_n = 53.48$ and 58.87 MHz) and Figure 5 ($f_n = 49.74$ MHz). The properties of the modes measured experimentally (Figures 4 and 5) are in agreement with those calculated numerically (Table 3). Indeed, having negligible normal component u_3 , eliminating compression wave radiation into adjacent liquid, the loss S_{12} measured for these modes with water loading (dashed) and without any liquid (solid) are almost equal each other ($S_{12}^{H_2O} \approx S_{12}^{air}$). Also, having large in-plane components (u_2 or u_1 and u_2), the same modes have high sensitivity towards viscosity (bold). Other modes (e.g., the mode detected at 48.5 MHz, Figure 5) have large normal component ($u_3/u_1 = 130$) and big radiation loss (>40 dB). These modes are useless for application.

Some modes from Table 4 are utilized for developing sensor prototypes. The calibration curves for one of them are shown on Figure 6. The curve for viscosity (Figure 6a) is typical for waves vibrating at ultrasonic frequencies [10]: it is almost linear for small η , when liquid behaves as ideal (Newtonian), and saturates for large η , when liquid behaves as a solid [10]. As a result, the sensitivity of the sensor is varied from 0.3 dB/cP for $\eta = 1$ –20 cP to 0.12 dB/cP for $\eta = 20$ –100 cP and 0.015 dB/cP for $\eta = 100$ –1500 cP.

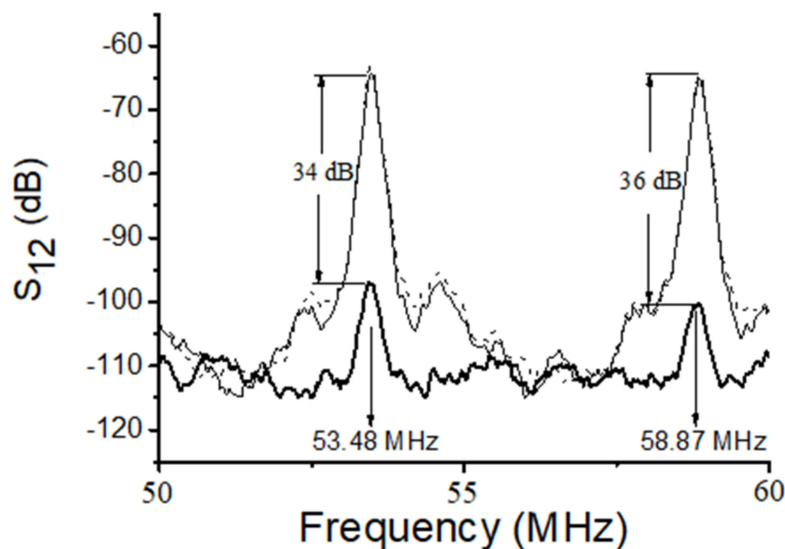


Figure 4. Insertion loss S_{12} of the SH-modes with high sensitivity towards viscosity measured at $h = 300 \mu\text{m}$, $\lambda = 300 \mu\text{m}$, and $h/\lambda = 1.0$ in ST,X + 90°-quartz plate with two free faces (thin solid), one free face, one water-loaded face (dashed), and one glycerin-loaded face (thick solid). Liquids are over the propagation path $L = 22 \text{ mm}$ on the bottom of the plate.

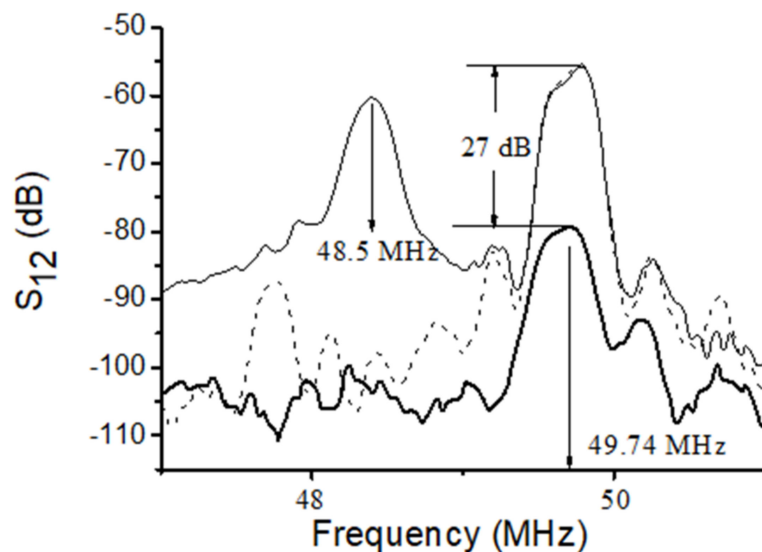


Figure 5. Insertion loss S_{12} of the Lamb modes with large radiation loss (48.5 MHz) and with high sensitivity towards viscosity (49.74 MHz) measured at $h = 300 \mu\text{m}$, $\lambda = 300 \mu\text{m}$, and $h/\lambda = 1.0$ in ST,X-quartz plate with two free faces (thin solid), one water-loaded face (dashed), and one glycerin-loaded face (thick solid). Liquids are over the propagation path $L = 22 \text{ mm}$ on the bottom of the plate.

The calibration curve of the same sensor for conductivity σ (Figure 6b) is also typical [22]: the electric response increases for small $\sigma < 0.4 \text{ S/m}$, approaches maximum at $\sigma = 0.4 \text{ S/m}$, and falls down to zero for large $\sigma > 1 \text{ S/m}$, when sensor becomes insensitive to liquid conductivity. Moreover, as the coupling coefficients of the modes from the Table 3 are small ($< 0.02\%$), the largest electric response (Figure 6b) is much lower than that is for viscosity (Figure 6a). The two responses become comparable with each other only for liquids with very small viscosities $\eta < 2 \text{ cP}$.

The temperature sensitivity of the same prototype without liquid loading (AIR) is negligible, but when a liquid is present, the prototype responds to the temperature accordingly to temperature dependence of the liquid viscosity (Figure 6c). Extracting the data for

unloaded plate from the data for plate with test liquid allows measuring the temperature dependence of viscosity $\eta(T)$ for the liquid. As an example, Figure 7 shows the as-measured (open rings) and the tabulated (black squares [39]) data for glycerin. It is seen both data are in agreement with one another.

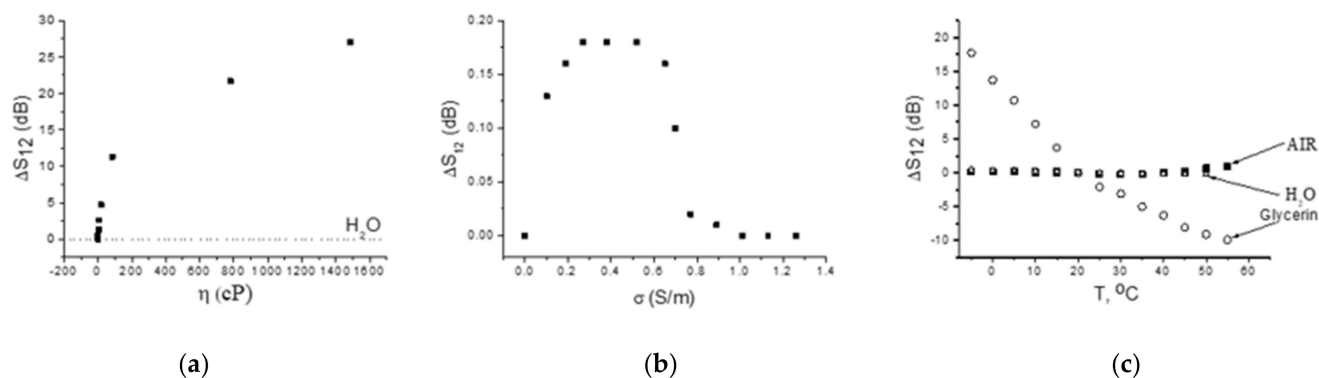


Figure 6. Calibration curves of the sensor prototype for viscosity (a), electric conductivity (b), and temperature (c) for ST,X-quartz plate, $h/\lambda = 1.0$, mode frequency 49.74 MHz. Liquids are over the propagation path $L = 22$ mm on the bottom of the plate.

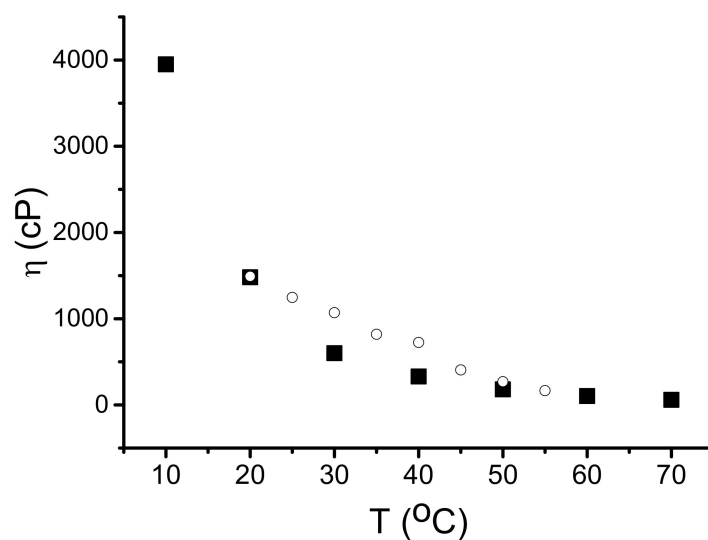


Figure 7. Temperature dependence of glycerin viscosity measured in the paper (circulars) by using Lamb mode with frequency 49.74 MHz in ST,X-quartz plate with $h/\lambda = 1.0$ and the same dependence taken from [39] (squares). Precision of our measurements is $\pm 20\%$.

The view of sensing element located in holder is shown on Figure 2b. Three pairs of interdigital transducers located on the bottom of quartz plate are visible through the plate thickness. Test liquid is deposited in central part of the top surface between transducers.

4. Conclusions

Modified Lamb and SH acoustic plate waves with increased sensitivity to liquid viscosity together with decreased sensitivity to liquid conductivity and temperature are found in quartz plates with thickness h of about wavelength λ . The modes are characterized by small or zero surface-normal displacement, avoiding mode radiation into adjacent liquid, and by large in-plane displacements, enhancing viscous coupling the wave and liquid deposited on the plate.

Basing on the waves with in-plane polarization, selective viscosity sensors are developed: sensitivity of the sensors towards viscosity is 0.3 dB/cP for 1–20 cP, 0.12 dB/cP for 20–100 cP, and 0.015 dB/cP for 100–1500 cP; responses towards conductivity (0 to 2 S/m) are two orders of magnitude smaller; temperature responses are almost zero in air, but when plate is coated with liquid they increase depending on liquid properties. Temperature dependence of glycerin viscosity measured by the sensor is in agreement with published data [39].

Author Contributions: Conceptualization, V.A. and I.K.; methodology, V.A.; software, P.L. and I.K.; validation, B.W.; investigation, E.S., F.Z., V.A., I.K.; writing—original draft preparation, V.A., I.K., Z.Q.; writing—review and editing, V.A., I.K., Z.Q.; visualization, E.S., I.K. All authors have read and agreed to the published version of the manuscript.

Funding: This research was funded by Russian Science Foundation, grant number 21-49-00062 and National Natural Science Foundation of China, grant number 1201101426.

Institutional Review Board Statement: Not applicable.

Informed Consent Statement: Not applicable.

Acknowledgments: Authors thanks the Acoustoelectronics and Piezoelectrics ELPA Corporation, Moscow, Russia for fabricating lithography masks and experimental samples.

Conflicts of Interest: The authors declare no conflict of interest.

References

- Gill, S.; Rowntree, A. Liquid lubricants for spacecraft applications. In *Chemistry and Technology of Lubricants*; Mortier, R.M., Fox, M.F., Orszulik, S.T., Eds.; Springer: Dordrecht, The Netherlands, 2010; pp. 375–387. [\[CrossRef\]](#)
- Mehta, D.M.; Kundu, P.; Chowdhury, A.; Lakhiani, V.K.; Jhala, A.S. A review of critical evaluation of natural ester vis-à-vis mineral oil Insulating liquid for use in transformers: Part II. *IEEE Trans. Dielect. Electr. Insul.* **2016**, *23*, 1705–1712. [\[CrossRef\]](#)
- Kalus, M.-R.; Lanyumba, R.; Barcikowski, S.; Gökce, B. Discrimination of ablation, shielding, and interface layer effects on the steady-state formation of persistent bubbles under liquid flow conditions during laser synthesis of colloids. *J. Flow Chem.* **2021**, *11*, 773–792. [\[CrossRef\]](#)
- Eaton, T.E.; Cox, D.A.; Barker, A.V. Sustainable production of marigold and calibrachoa with organic fertilizers. *HortScience* **2013**, *48*, 637–644. [\[CrossRef\]](#)
- Santos, J.; Calero, N.; Guerrero, A.; Muñoz, J. Relationship of rheological and microstructural properties with physical stability of potato protein-based emulsions stabilized by guar gum. *Food Hydrocoll.* **2015**, *44*, 109–114. [\[CrossRef\]](#)
- Murray, B.S. Rheological properties of protein films. *Curr. Opin. Colloid Interface Sci.* **2011**, *16*, 27–35. [\[CrossRef\]](#)
- Jenkinson, I.R.; Sun, X.X.; Seuront, L. Thalassorheology, organic matter and plankton: Towards a more viscous approach in plankton ecology. *J. Plankton Res.* **2015**, *37*, 1100–1109. [\[CrossRef\]](#)
- Chen, C.-J.; Chen, W.-L.; Pham, H.P.; Chuang, H.-S.; Chen, G.; Zhao, L.; Liu, Y.; Liao, F.; Han, D.; Zhou, H. Regulation of blood viscosity in disease prevention and treatment. *Chin. Sci. Bull.* **2012**, *57*, 1946–1952. [\[CrossRef\]](#)
- Ballantine, D.S.; White, R.M.; Martin, S.J.; Ricco, A.J.; Zeller, E.T.; Frye, G.C.; Wohltjen, H. Acoustic wave sensors and responses. In *Acoustic Wave Sensors*; Academic Press: San Diego, CA, USA, 1997.
- Ricco, A.J.; Martin, S.J. Acoustic wave viscosity sensor. *Appl. Phys. Lett.* **1987**, *50*, 1474–1476. [\[CrossRef\]](#)
- Bury, P.; Cernobola, F.; Veverick, M.; Kudelcik, J.; Hardon, S.; Rajnak, M.; Pavlovicova, K.; Timko, M.; Kopcansky, P. Investigation of structural changes in oil-based magnetic fluids by surface acoustic waves. *J. Magn. Magn. Mater.* **2020**, *501*, 166392. [\[CrossRef\]](#)
- Nomura, T.; Saitoh, A.; Horikoshi, Y. Measurement of acoustic properties of liquid using liquid flow SH-SAW sensor system. *Sens. Actuators B Chem.* **2001**, *76*, 69–73. [\[CrossRef\]](#)
- Lindner, G. Sensors and actuators based on surface acoustic waves propagating along solid–liquid interfaces. *J. Phys. D Appl. Phys.* **2008**, *41*, 123002. [\[CrossRef\]](#)
- Mitsakakis, K.; Tsortos, A.; Kondoh, J.; Gizeli, E. Parametric study of SH-SAW device response to various types of surface perturbations. *Sens. Actuators B* **2009**, *138*, 408–416. [\[CrossRef\]](#)
- Kondoh, J.; Nakayama, K.; Kuznetsova, I. Study of frequency dependence of shear horizontal surface acoustic wave sensor for engine oil measurements. *Sens. Actuators A Phys.* **2021**, *325*, 112503. [\[CrossRef\]](#)
- Nomura, T.; Yasuda, T. Measurement of velocity and viscosity of liquid using surface acoustic wave delay line. *Jpn. J. Appl. Phys.* **1990**, *29*, 140. [\[CrossRef\]](#)
- Deng, L.; Bao, L.; Wei, W.; Nie, L.; Yao, S. Rapid bacteria detection based on gelatin liquefaction with a piezoelectric viscosensor. *Instrum. Sci. Technol.* **1997**, *25*, 69–80. [\[CrossRef\]](#)
- Ju, S.; Zhang, C.; Zahedinejad, P.; Zhang, H. SC-Cut quartz resonators for dynamic liquid viscosity measurements. *IEEE Trans. on Ultras. Ferroel. Freq. Control* **2021**, *68*, 3616–3623. [\[CrossRef\]](#)

19. Lévêque, G.; Ferrandis, J.Y.; Van Est, J.; Cros, B. An acoustic sensor for simultaneous density and viscosity measurements in liquids. *Rev. Sci. Instrum.* **2000**, *71*, 1433–1440. [[CrossRef](#)]
20. Patois, R.; Vairac, P.; Cretin, B. Near-field acoustic densimeter and viscosimeter. *Rev. Sci. Instrum.* **2000**, *71*, 3860. [[CrossRef](#)]
21. Borodina, I.; Zaitsev, B.; Teplykh, A. The influence of viscous and conducting liquid on the characteristics of the slot acoustic wave. *Ultrasonics* **2018**, *82*, 39–43. [[CrossRef](#)]
22. Zaitsev, B.; Kuznetsova, I.; Joshi, S.; Borodina, I. Acoustic waves in piezoelectric plates bordered with viscous and conductive liquid. *Ultrasonics* **2001**, *39*, 45–50. [[CrossRef](#)]
23. Kazys, R.; Sliteris, R.; Raisutis, R.; Zukauskas, E.; Vladisauskas, A.; Mazeika, L. Waveguide sensor for measurement of viscosity of highly viscous fluids. *Appl. Phys. Lett.* **2013**, *103*, 204102. [[CrossRef](#)]
24. Gitis, A.; Sauer, D.U. The propagation of horizontally polarized shear waves in plates bordered with viscous liquid. *Ultrasonics* **2016**, *71*, 264–270. [[CrossRef](#)] [[PubMed](#)]
25. Teston, F.; Tessier, L.; Feuillard, G.; Richard, E.; Roncin, A.; Lethiecq, M. The multi-layered effective permittivity function applied to the mass loading and viscous coupling in shear horizontal-acoustic plate modes. *Sens. Actuators B Chem.* **1999**, *59*, 171–176. [[CrossRef](#)]
26. Andle, J.; Haskell, R.; Sbardella, R.; Morehead, G.; Chap, M.; Columbus, J.; Stevens, D. Design, Optimization and Characterization of an Acoustic Plate Mode Viscometer. In Proceedings of the IEEE Sensors 2007 Conference, Atlanta, GA, USA, 28–31 October 2007; pp. 864–867. [[CrossRef](#)]
27. Sun, J.; Du, J.; Yang, J.; Wang, J. Shear-horizontal waves in a rotated Y-cut quartz plate in contact with a viscous liquid. *Ultrasonics* **2012**, *52*, 133–137. [[CrossRef](#)] [[PubMed](#)]
28. Anisimkin, V.; Caliendo, C.; Verona, E. Acoustic Plate Mode sensing in liquids based on free and electrically shorted plate surfaces. *Ultrasonics* **2016**, *68*, 29–32. [[CrossRef](#)]
29. Anisimkin, V.I.; Kuznetsova, I.E. Selective detection of micro liquid probes temperature using surface acoustic waves. *J. Commun. Technol. Electron.* **2019**, *64*, 831–834. [[CrossRef](#)]
30. Anisimkin, I.V.; I Anisimkin, V. Attenuation of acoustic normal modes in piezoelectric plates loaded by viscous liquids. *IEEE Trans. Ultrason. Ferroelectr. Freq. Control* **2006**, *53*, 1487–1492. [[CrossRef](#)]
31. Zaitsev, B.D.; Shikhabudinov, A.M.; Teplykh, A.A.; Kuznetsova, I.E. Liquid sensor based on a piezoelectric lateral electric field-excited resonator. *Ultrasonics* **2015**, *63*, 179–183. [[CrossRef](#)]
32. Rostami, A.; Kaatuzian, H.; Rostami-Dogolsara, B. Acoustic 1×2 demultiplexer based on fluid-fluid phononic crystal ring resonators. *J. Mol. Liq.* **2020**, *308*, 113144. [[CrossRef](#)]
33. Wang, T.-T.; Wang, Y.-F.; Deng, Z.-C.; Laude, V.; Wang, Y.-S. Reconfigurable waveguides defined by selective fluid filling in two-dimensional phononic metaplates. *Mech. Syst. Signal Process.* **2021**, *165*, 108392. [[CrossRef](#)]
34. Zaki, S.E.; Mehaney, A.; Hassanein, H.M.; Aly, A.H. High-performance liquid sensor based one-dimensional phononic crystal with demultiplexing capability. *Mater. Today Commun.* **2021**, *26*, 102045. [[CrossRef](#)]
35. Anisimkin, V.; Voronova, N. New modification of the acoustic Lamb waves and its application for liquid and ice sensing. *Ultrasonics* **2021**, *116*, 106496. [[CrossRef](#)] [[PubMed](#)]
36. Adler, E.; Farnell, G.; Slaboszewicz, J.; Jen, C. Interactive PC software for SAW propagation in anisotropic multilayers. In Proceedings of the IEEE 1988 Ultrasonics Symposium, Chicago, IL, USA, 2–5 October 1988; pp. 103–107. [[CrossRef](#)]
37. Kuznetsova, I.E.; Zaitsev, B.D.; Joshi, S.G.; Teplykh, A. Effect of a liquid on the characteristics of antisymmetric lamb waves in thin piezoelectric plates. *Acoust. Phys.* **2007**, *53*, 557–563. [[CrossRef](#)]
38. Slobodnik, A.J.; Conway, E.D.; Delmonico, R.T. *Microwave Acoustic Handbook*; Air Force Cambridge Research Laboratories: Bedford, MA, USA, 1973; AFCRL198 TR-73-0597.
39. Weast, R.C. *Chemical Rubber Company Handbook of Chemistry and Physics*, 66th ed.; Chemical Rubber: Boca Raton, FL, USA, 1985; p. D254.
40. Murav'eva, O.V.; Murav'ev, V.V.; Zlobin, D.V.; Bogdan, O.P.; Syakterev, V.N.; Volkov, V.V. Technique and device for the experimental estimation of the acoustic impedance of viscoelastic medium. *Devices Methods Meas.* **2017**, *8*, 314–326.
41. Caliendo, C.; D'Amico, A.; Verardi, P.; Verona, E. K/sup +/- detection using shear horizontal acoustic modes. *IEEE Symp. Ultrason.* **1991**, *1*, 383–387. [[CrossRef](#)]
42. Anisimkin, I.V. New type of an acoustic plate mode: Quasi-longitudinal normal wave. *Ultrasonics* **2004**, *42*, 1095–1099. [[CrossRef](#)]
43. Anisimkin, V.I.; Voronova, N.V.; Puchkov, Y.V. General properties of the acoustic plate modes at different temperatures. *Ultrasonics* **2015**, *62*, 46–49. [[CrossRef](#)]